RESEARCH ARTICLE

Macromolecular Chemistry and Physics
www.mcp-journal.de

The Decisive Role of Confinement in Enhancing or Suppressing Self-Nucleation in Polyethylene-Containing Block Copolymers

Yilong Liao, Leire Sangroniz, Maryam Safari, Holger Schmalz, and Alejandro J. Müller**

The influence of confinement on the self-nucleation behavior of crystallizable polyethylene (PE) and poly(ethylene oxide) (PEO) blocks in block copolymers of different architectures is studied by differential scanning calorimetry. The amorphous blocks, polystyrene (PS) and poly(methyl methacrylate) (PMMA), with high glass transition temperatures, create glassy matrices that confine crystallization in the microphase-segregated block copolymers. For diblock copolymers (PS-*b*-PE, PMMA-*b*-PE), the PE blocks exhibit stronger melt memory than neat PE, as moderate confinement favors the preservation of the conformations adopted in the crystalline regions. However, when both ends of the PE block are tethered to glassy blocks, in PS-*b*-PE-*b*-PS and PS-*b*-PE-*b*-PMMA, melt memory and self-nucleation completely vanish as the confinement degree increases. In PS-*b*-PE-*b*-PEO triblock terpolymers, the self-nucleation of the PE block is hindered even at very low temperatures, where annealing is dominant. The PEO block undergoes a complex fractionated crystallization where self-nucleation disappears in the isolated, highly confined microdomains. SSA (successive self-nucleation and annealing) thermal fractionation results are similar for PE homopolymer and PE blocks (i.e., hydrogenated polybutadiene), resulting from molecular defects caused by branching. These results indicate that the melt memory of confined crystallizable blocks can be triggered by moderate confinement but is completely suppressed when confinement is too strong.

1. Introduction

Well-defined block copolymers containing amorphous blocks and at least one crystallizable block are interesting materials because they exhibit two self-organizing mechanisms driven by microphase separation and crystallization.[1–3] A competition between the driving force of crystallization and microphase segregation will define their final solid-state morphology.[2,4–11] In addition, next to the segregation strength quantified by the Flory–Huggins interaction parameter χ and the block copolymer composition, the relative magnitudes of three critical transition temperatures play a pivotal role in determining the final morphology of block copolymers: The order-disorder transition temperature (T_{ODT}), the glass transition temperature (T_g) of the amorphous block, and the crystallization temperature (T_c) of the crystallizable block.[12,13]

In the case of $T_c > T_g$, two scenarios are possible. In the first scenario, T_c is also greater than T_{ODT}. In this case, the crystallization process is similar to that starting in a homogeneous melt, with the crystallization process driving microphase

Y. Liao, L. Sangroniz, A. J. Müller
POLYMAT and Department of Polymers and Advanced Materials: Physics Chemistry and Technology
Faculty of Chemistry
University of the Basque Country UPV/EHU
Paseo Manuel de Lardizábal, 3, Sebastián, Donostia-San 20018, Spain
E-mail: alejandrojesus.muller@ehu.es

M. Safari
Aachen-Maastricht Institute for Biobased Materials (AMIBM)
Maastricht University
Urmonderbaan 22, Geleen 6167 RD, The Netherlands

H. Schmalz
Macromolecular Chemistry
University of Bayreuth
Universitätsstraße 30, 95447 Bayreuth, Germany
E-mail: holger.schmalz@uni-bayreuth.de

H. Schmalz
Bavarian Polymer Institute (BPI)
University of Bayreuth
Universitätsstraße 30, 95447 Bayreuth, Germany

A. J. Müller
IKERBASQUE
Basque Foundation for Science
Plaza Euskadi 5, Bilbao 48009, Spain

The ORCID identification number(s) for the author(s) of this article can be found under https://doi.org/10.1002/macp.202500056

DOI: 10.1002/macp.202500056

separation. The resulting microdomain (MD) morphology is typically lamellar, where the crystalline lamellae are sandwiched between amorphous layers.[14–16] In contrast, a so-called "soft confinement" condition arises when T_{ODT} exceeds T_c.[12,13,17] Here, the segregation strength determines the final MD morphology.[8,14] Breakout crystallization dominates for systems with weak segregation strength, disrupting any pre-existing phase-segregated morphology observed in the molten state. This often leads to the formation of lamellar structures, where polymer chains reorganize in different ways depending on the composition. In contrast, the MD morphology depends on composition for strongly segregated systems and remains confined.[15] In this last case, crystallization has to occur confined within the microphase-segregated morphology dictated by composition: spheres, cylinders, lamellae, etc.

When $T_{ODT} > T_g > T_c$, the amorphous block becomes glassy before crystallization occurs. When the crystallizable block is the minority component, the crystallizable block is confined within a small isolated MD, leading to confined crystallization.[4,18–25] For example, when polyethylene (PE) is one of the crystallizable blocks, crystallization occurs from a phase-segregated melt in some diblock copolymers, such as PS-*b*-PE,[26,27] PE-*b*-P*L*LA, and PE-*b*-P*D*LA (PS = polystyrene, P*L*LA/P*D*LA = poly(L-lactide)/poly(L,D-lactide)).[28] This phenomenon occurs even in phase-segregated systems where the segregation strength is high or even intermediate because the presence of the glassy matrix restricts the crystallization of the MDs formed by microphase separation.

It is noted that the crystallizable PE blocks in the aforementioned block copolymers were produced through the hydrogenation of the corresponding block copolymer precursors containing poly(1,4-butadiene) (PB) blocks, which were obtained via sequential living anionic polymerization. This process resulted in "pseudo" PE blocks with a certain fraction of ethyl branches (arising from the residual 1,2-units in the polybutadiene blocks, typically 10–12 mol%) and, therefore, lower melting and crystallization temperatures than linear PE[22,29]

The development of metal-based coordination polymerization methods that enable precise stereochemical control in living olefin polymerization has facilitated access to block copolymers containing linear PE and stereoregular polyolefin blocks, revealing intriguing phenomena.[30–33] For instance, in double crystalline PE-*block*-isotactic polypropylene (PE-*b*-*i*PP) block copolymers, crystallization can either be confined, or breakout crystallization can occur depending on the rate used for cooling from the melt. Furthermore, epitaxial crystallization onto a benzoic acid crystal substrate can disrupt the phase-separated structure in the melt, inducing the formation of ordered lamellar nanostructures with alternating layers of *i*PP and PE[34] Generally, the final morphology created by epitaxial crystallization onto a substrate depends on which block, PE or the stereoregular PP, crystallizes first, a process influenced by composition and molecular weight.[35] This indicates that crystalline block copolymers provide the opportunity to create precise nanoscale patterns, enabling control over both the microstructure of block copolymers and the alignment of microdomains.

One straightforward approach to studying the influence of confinement on the nucleation and crystallization of crystallizable blocks is the self-nucleation (SN) protocol employing differential scanning calorimetry (DSC).[3,15,36–40] The SN protocol starts by creating a standard semi-crystalline history in a crystallizable polymer by cooling the material from the isotropic melt at a constant cooling rate down to a temperature at which the crystallization has already occurred. Then, this semi-crystalline polymer, with a standard thermal history, is heated to a given self-nucleation temperature (T_s), where it remains for a fixed amount of time (usually 3 or 5 min). Depending on the value of T_s, three SN *Domains* can be defined.[36,41–46]

In *Domain I* (*DI*), also known as the "*melting Domain*", T_s is high enough to erase all thermal history, resulting in an isotropic melt. In the subsequent cooling from this isotropic melt, the peak crystallization temperature (T_c) does not vary with the selected T_s temperature as only temperature-resistant heterogeneities remain active in the material (i.e., heterogeneous nucleation). As T_c is proportional to the nucleation density of active nuclei in the sample, no self-nucleation occurs within *Domain I*.

In *Domain II* (*DII*), known as the "*self-nucleation Domain*", T_s is lower than in *DI* and capable of producing self-nuclei within the sample that, upon cooling from T_s, will cause a SN effect characterized by an increase in T_c. Müller et al.[41,42] proposed a division of *DII* into two distinct sub-*Domains*. *Domain IIa* (*DIIa*) or "*melt memory Domain*" occurs at high T_s values within *DII*. In *DIIa*, T_s is high enough to melt all crystals but low enough to produce some "self-nuclei" whose exact nature is under debate. However, it is a fact that they can self-nucleate the polymer during subsequent cooling from T_s. This phenomenon is termed melt memory (as no crystals are involved). Even after the material surpasses the melting point of all crystals, it can still retain a memory of the chain conformations from their previous crystallographic arrangement or a residual chain orientation that persists within the melt. So, upon cooling from a self-nucleated melt in *DIIa*, these regions in the melt or self-nuclei provoke a SN effect. The melt memory is triggered by intermolecular interactions in the crystals, and its survival rate increases with entanglement density, i.e., increasing molecular weight.[42]

Domain IIb, or the "*self-seeding Domain*", occurs in the lower temperature region of *DII*. T_s is high enough to melt most crystals, but crystal fragments survive (but they do not anneal during the holding time at *DIIb*) and constitute self-seeds that can nucleate the polymer epitaxially.

Finally, in *Domain III* (*DIII*), termed the "*self-nucleation and annealing Domain*", T_s is too low and only provokes partial melting of the polymer crystals. The remaining crystals anneal (thicken) during the holding time at T_s. When the sample is cooled, the molten part of the material self-nucleates on the unmelted crystals present.

The classical SN behavior of crystallizable blocks within block copolymers, i.e., displaying the three types of SN *Domains*, has been observed in weakly segregated block copolymers or those forming a miscible melt, or when the segregated crystalline phases are percolated, as reported for interconnected lamellar or cylindrical morphologies.[15,39,47] However, when the crystallizable block forms isolated MDs, the nucleation process becomes confined within each MD. The disappearance of the *self-nucleation Domain* (*DII*) has been observed in systems where the crystallizable block, such as PE, poly(ethylene oxide) (PEO), or poly(ϵ-caprolactone) (PCL), is confined and isolated within

MDs like cylinders and spheres.[3,15,38,39,48] This phenomenon could be attributed to the significantly larger number of MDs compared to the self-nuclei generated or to the macromolecular topological effects imposed by strong confinement.[38,49] Although block copolymers provide an excellent confined environment, their MD sizes cannot be adjusted over a wide range while maintaining a consistent morphology. Wang et al. effectively addressed this issue using anodized aluminum oxide (AAO) templates with controllable dimensions.[50] They discovered that both poly(butylene succinate) and PCL homopolymers completely lose their *Domain II* when infiltrated within AAO with diameters smaller than 60 nm. Interestingly, Balsamo et al.[38] observed not only the absence of *DII* in a PS-*b*-PE-*b*-PCL ABC triblock terpolymer but also the lack of SN in *DIII*, where crystallite annealing had already occurred. In some cases, an even lower T_s within *DIII* was required to induce SN of the confined crystallizable blocks. Consequently, *Domain III* had to be divided into a purely *annealing Domain* ($DIII_A$), where only annealing occurs without SN, and $DIII_{SA}$, where traditional SN and annealing occur simultaneously.

In previous work, we investigated the morphology and confined crystallization behavior of the PE block in different di- (AB) and triblock (ABA and ABC) copolymers, where the amorphous blocks consisted of PS and/or poly(methyl methacrylate) (PMMA).[51] The topological confinement imposed by the covalent linkage of PE to other blocks (such as glassy PS and PMMA or crystallizable PEO), combined with the morphological confinement within distinct PE microdomains (e.g., cylinders or lamellae), significantly impacts the crystallization behavior. Strong confinement effects were observed in triblock terpolymers where the PE lamellae are "disrupted" by PS cylinders or distorted PS microdomains. This disruption leads to significantly reduced crystallization temperatures and degrees of crystallinity compared to other block copolymers studied. Although the influences of block length, number, and composition on crystallization and morphology have been extensively investigated, the SN behavior remains undisclosed.

In this work, we examine the influence of confinement on the SN behavior of the aforementioned di- and triblock copolymers with a common crystallizable PE block (**Scheme 1**). The diblock

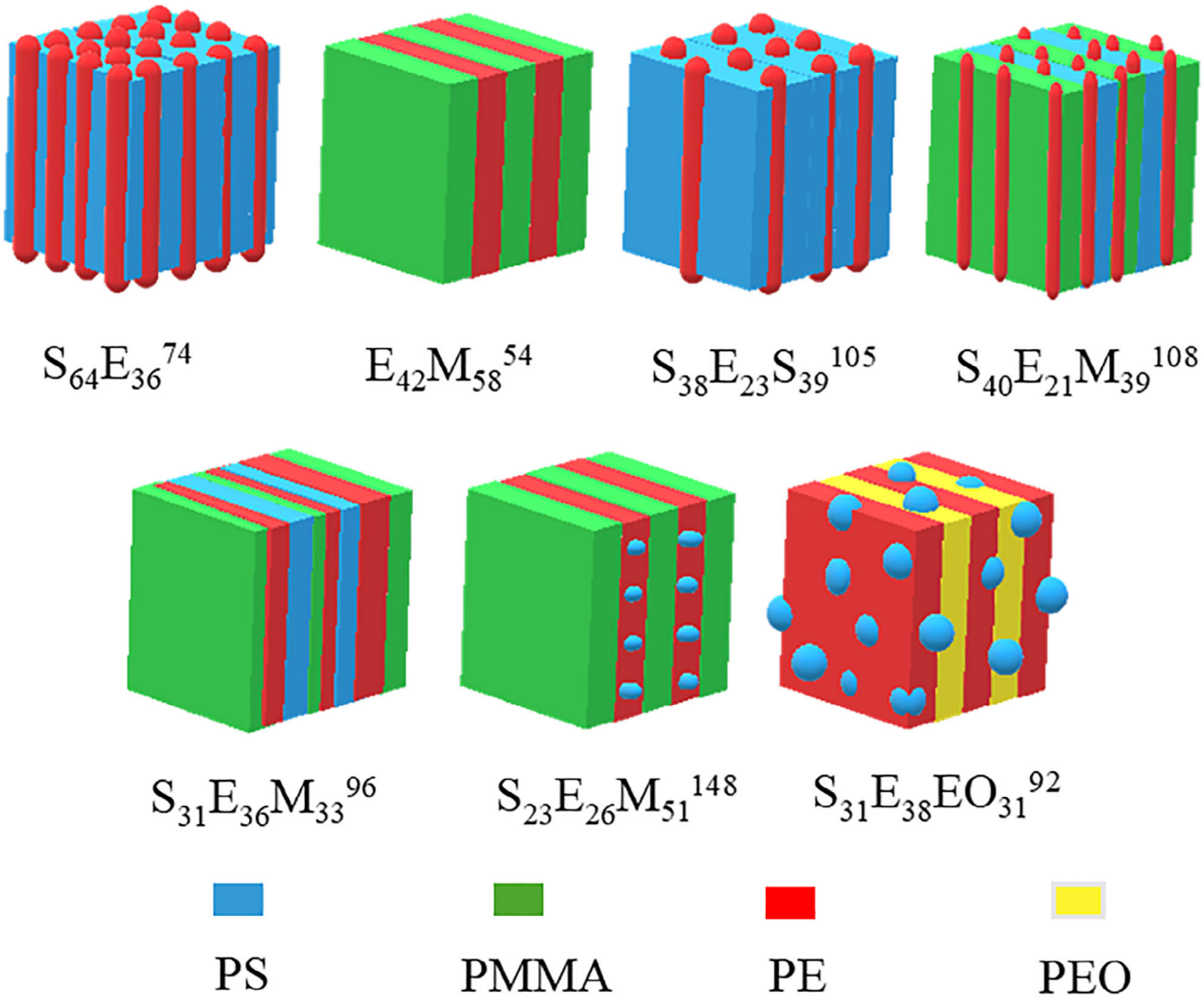

Scheme 1. Schematic cartoon of the studied block copolymer morphologies.

Table 1. Molecular characteristics and morphology of the studied block copolymers.

Sample[a)]	PB-containing precursor[a)]	1,4-PB[b)] [mol%]	$Đ$	Morphology[c)]	Remark
$E_{42}M_{58}{}^{54}$	$B_{41}M_{59}{}^{53}$	87	1.05	Lamellar	Alternating PE/PMMA lamellae
$S_{64}E_{36}{}^{74}$	$S_{65}B_{35}{}^{73}$	91	1.03	Cylindrical	PE cylinders in PS matrix
$S_{38}E_{23}S_{39}{}^{105}$	$S_{38}B_{23}S_{39}{}^{105}$	89	1.04	Cylindrical	PE cylinders in PS matrix
$S_{40}E_{21}M_{39}{}^{108}$	$S_{40}B_{21}M_{39}{}^{107}$	89	1.03	Lamella-Cylinder	PE cylinders sandwiched between PS and PMMA lamellae
$S_{31}E_{36}M_{33}{}^{96}$	$S_{33}B_{34}M_{33}{}^{94}$	90	1.02	Lamella-Lamella,	PE lamellae sandwiched between PS and PMMA lamellae
$S_{23}E_{26}M_{51}{}^{148}$	$S_{23}B_{25}M_{52}{}^{147}$	87	1.03	Cylinder in Lamella-Lamella	PS cylinders in PE lamellae +PMMA lamellae
$S_{31}E_{38}EO_{31}{}^{92}$	$S_{32}B_{37}EO_{31}{}^{91}$	88	1.02	Distorted domains in Lamella-Lamella	Distorted PS domains in PE lamellae +PEO lamellae

The molecular characteristics and morphology of block copolymers have been investigated in our previous report.[51] [a)] Monomer abbreviations: S, styrene; E, ethylene; M, methyl methacrylate; B, butadiene (preferential 1,4-addition); EO, ethylene oxide. The subscripts represent the weight fraction (wt.%) of the respective block, while the superscript indicates the overall number-average molecular weight (M_n) of the block copolymer expressed in kg mol^{-1}; [b)] Mole fraction of 1,4-units in the PB block of the respective precursor block copolymer determined by proton nuclear magnetic resonance (^{1}H NMR); [c)] Morphologies of block copolymers were determined by transmission electron microscopy (TEM) and atomic force microscopy (AFM).

copolymers exhibit a remarkable melt-memory effect, with PS-*b*-PE even showing a stronger melt-memory effect than branched neat PE. However, in the case of triblock copolymers, the stronger confinement effect leads to the disappearance of the exclusive *self-nucleation Domain* (*DII*) due to the covalent bonding at both ends of the PE block. Interestingly, the confinement effects depend not only on the PE content, as it turned out that the final morphology of the block copolymer plays a more prominent role.

2. Experimental Section

2.1. Materials

The block copolymers studied were obtained by catalytic hydrogenation of the corresponding PB-containing block copolymers, which were synthesized through sequential living anionic polymerization. For example, the diblock copolymer PS-*b*-PE was prepared by hydrogenating the PS-*b*-PB diblock copolymer obtained via living anionic polymerization. The molecular characteristics and morphologies are summarized in **Table 1** and Scheme 1; more details can be found in the previous work.[51]

2.2. Differential Scanning Calorimetry (DSC)

Thermal analysis was performed on a PerkinElmer 8000 calorimeter with an Intracooler 2P cooling system. The materials were heated and cooled at 20 °C min^{-1} for a preliminary thermal characterization. Before measurement, the samples were held in the melt at either 150 °C or 100 °C (PS-*b*-PB-*b*-PEO precursor) for 3 min to eliminate any prior thermal history.

2.2.1. Self-Nucleation (SN) Experiments

The typical thermal program of SN is shown in **Scheme 2a**, which was proposed by Fillon et al.[36] and extensively used and reviewed by Müller et al.[41,42] It consisted of five steps at a scanning rate of 20 °C min^{-1}:

1) The sample was heated to a sufficiently high temperature to erase any thermal history, usually T_m + 25 °C, and was held at this temperature for 3 min to achieve an isotropic melt.
2) The isotropic melt was cooled to a minimum temperature of −40 °C at 20 °C min^{-1} and then held for 1 min to establish a standard semi-crystalline state. The exothermic peak observed during cooling is defined as the "standard" crystallization temperature (T_c). Once the cooling rate and the initial and final temperatures were fixed, this standard state could be consistently reproduced in any SN experiment.
3) The standard crystalline sample was heated to a self-nucleation temperature (T_s) lower than the temperature used to erase thermal history and held at this temperature for 5 min for thermal conditioning. In classical SN behavior, the standard crystalline sample could undergo complete melting, self-nucleation only, or self-nucleation and annealing, depending on the applied T_s. Accordingly, the well-known three *Domains* were identified: *Domain I*, also called the "*melting Domain*"; *Domain II*, known as the "*self-nucleation Domain*"; and *Domain III*, or the *self-nucleation and annealing Domain*. However, in the previous works on block copolymers,[31] in some cases, annealing occurred without SN in *Domain III*. To distinguish such cases, this *sub-Domain* is defined as *Domain* III_A ($DIII_A$), while the conventional *Domain III* is denoted *Domain* III_{SA} ($DIII_{SA}$).
4) A subsequent cooling scan from T_s to the minimum temperature chosen in step 2 was recorded by DSC to assess the SN effect.
5) Finally, the sample was heated until the isotropic melt state was achieved (as in step 1), and its melting behavior was recorded.

2.2.2. Successive Self-Nucleation and Annealing (SSA) Experiments

SSA is a thermal fractionation technique developed by Müller et al.[44,46,52–54] that enhances the molecular fractionation that can occur during crystallization and promotes the annealing of unmelted crystals at each process stage.

As shown in Scheme 2b, the first stages of SSA are the same as in steps 1–4, described in the SN protocol. Special care should be taken when choosing the first T_s temperature used in step 3. The first T_s should be the lowest temperature in *DII*, also known as $T_{s,\,ideal}$. This temperature generates the highest density of self-

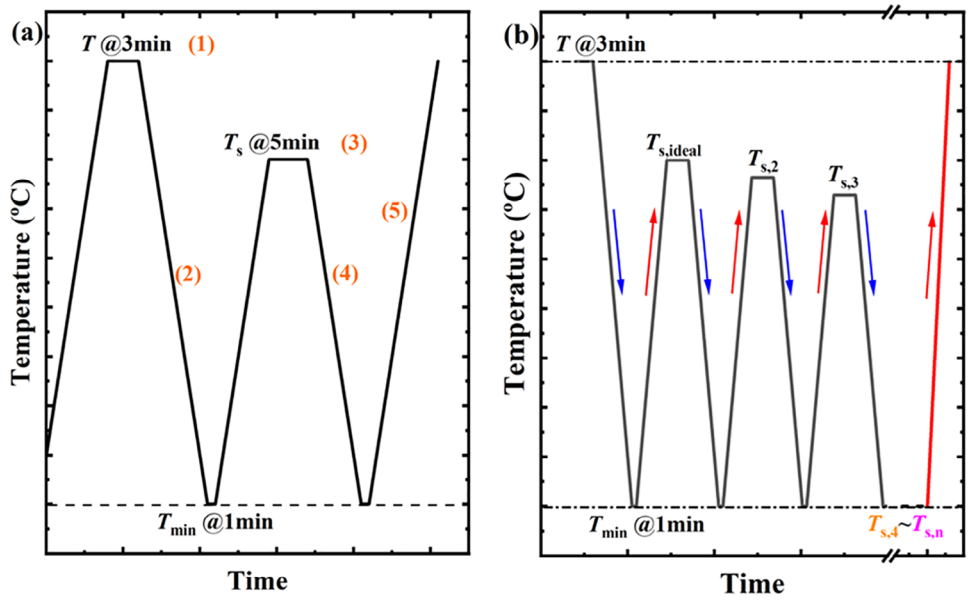

Scheme 2. Schematic representations of a) SN and b) SSA protocols.

nuclei without any annealing of unmelted crystals. The sample is then reheated to $T_{s,2}$, which is 5 °C below the $T_{s,ideal}$, and held for 5 min to fractionate the polymer. Since $T_{s,2}$ is in *DIII*, the unmelted crystals were annealed, and the molten polymer was self-nucleated. Meanwhile, isothermal crystallization will also occur during the 5 min fractionation time. As a result, the thermal fraction 1 (highest melting peak) was generated and "refined" by the subsequent cyclic treatments applied. Note that the fractionation window of 5 °C and the annealing time of 5 min remain constant throughout the SSA treatment.

The aforementioned thermal fractionation steps were repeated at progressively lower T_s until the entire width of the endothermic peak was spanned. Finally, the last DSC heating scan after SSA revealed a distribution of endothermic peaks caused by the previous fractionation treatment.

3. Results and Discussion

3.1. Thermal Properties of Block Copolymers and Their Dependence on PE Content

Figure 1 illustrates the variation of thermal parameters for all samples as a function of the weight fraction of PE in the block copolymers. These parameters include T_c (obtained from DSC cooling scans from the isotropic melt), T_m (obtained from subsequent DSC heating curves), and enthalpy values corresponding to these processes. The DSC curves from which these data were obtained are reported in the Supporting Information (Figure S1, Supporting Information).

The data on a reference neat PE, obtained by hydrogenation of a PB homopolymer with a high molar fraction of 1,4-units (1,4-PB, 89 mol%), is also included in Figure 1. As the reference PE and the PE blocks within the block copolymers are hydrogenated PBs, their calorimetric properties will be a function of the short-chain branching content (which comes from the residual 1,2-units in the PB precursor). Table 1 lists the 1,4-PB content of the samples. The higher the fraction of 1,4-PB units in the precursors, the higher the values expected for the material's first-order transitions (T_c and T_m) when considered as pure phases (i.e., in the absence of confinement).

Figure 1 shows, as a general trend, that when the PE content in the block copolymers decreases, both T_c and T_m exhibit a pronounced decrease. This can be attributed to the effects of confinement exerted on the PE block within MDs of increasingly reduced dimensions. For comparison, the respective morphologies displayed by the samples, as determined in our previous work employing AFM and TEM[41] are summarized in Scheme 1. The two arrows in Figure 1a are lines to guide the eye and indicate the global trend observed. One exception to the trend is the $S_{64}E_{36}{}^{74}$ diblock copolymer, which exhibits higher T_c and T_m compared to $E_{42}M_{58}{}^{54}$ despite its lower PE fraction. The reason for this behavior is its lower amount of short-chain branches, as reported in Table 1 (i.e., a higher amount of 1,4-units in the PB precursor).

Figure 1a also shows that although $S_{31}E_{36}M_{33}{}^{96}$ has the same PE content as $S_{64}E_{36}{}^{74}$, the T_c and T_m of the triblock terpolymer are significantly lower than those of the diblock copolymer. This is attributed to the stronger confinement imposed on the PE blocks within the SEM triblock terpolymer, as both ends are covalently linked to glassy PS and PMMA blocks. The T_g values of both PS and PMMA blocks (≈100 and 110 °C) are higher than T_c of the PE block (always well below 90 °C, depending on the sample, see Figure 1a), thus imposing a hard confinement effect in the SEM triblock terpolymer. Please note that the PE blocks in the case of these two samples ($S_{64}E_{36}{}^{74}$ and $S_{31}E_{36}M_{33}{}^{96}$) have nearly the same 1,4-units content (91 and 90 mol%, Table 1) in the respective PB precursors, or in other words, similar short-chain branch content. Therefore, the reason for the first-order transition temperature depression in the triblock terpolymer compared to the diblock copolymer can be attributed to the confinement ef-

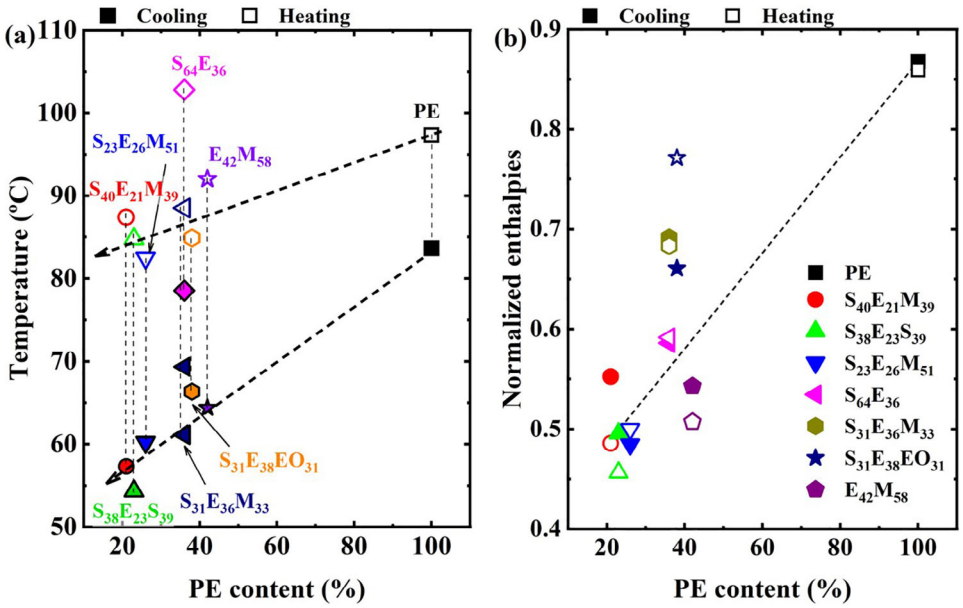

Figure 1. a) T_c and T_m and b) normalized enthalpies by PE fraction as a function of PE content. The results of neat PE are presented as a reference. The solid symbols indicate the parameters obtained during cooling, while the open symbols correspond to the heating process. The observed BCP morphologies (Table 1) are listed below for clarity. $E_{42}M_{58}$[54]: alternating PE/PMMA lamellae; $S_{64}E_{36}$[74] and $S_{38}E_{23}S_{39}$[105]: PE cylinders in PS matrix; $S_{40}E_{21}M_{39}$[108]: PE cylinders sandwiched between PS and PMMA lamellae; $S_{31}E_{36}M_{33}$[96]: PE lamellae sandwiched between PS and PMMA lamellae; $S_{23}E_{26}M_{51}$[148]: PS cylinders in PE lamellae + PMMA lamellae; $S_{31}E_{38}EO_{31}$[92]: distorted PS domains in PE lamellae + PEO lamellae.

fect of having the PE block chains tethered on both ends to chemically different glassy amorphous blocks. Accordingly, for the triblock copolymers $S_{23}E_{26}M_{51}$[148], $S_{38}E_{23}S_{39}$[105], and $S_{40}E_{21}M_{39}$[108], which have very similar PE contents, the fluctuations in their thermal parameters can be related to their unique morphology (see Scheme 1).[44]

In the case of the latent heat of crystallization and fusion (i.e., normalized enthalpies of crystallization and melting in Figure 1b), the PE block content plays a decisive role. This is reasonable, as a reduction in the PE block content inevitably leads to a change in morphology (with reduced PE MDs dimensions) and a concomitant increase in confinement degree, which causes the observed reduction in the amount of PE crystals formed. There is a good match between the enthalpies of crystallization and melting, as expected for adiabatic calorimetry measurements.

3.2. SN Behavior in Diblock Copolymers

Confinement significantly influences the melt memory of semicrystalline polymers. In this study, the constraints imposed on the PE block within diblock copolymers (with one chain end tethered covalently to a glassy block, i.e., PS or PMMA) are relatively weaker compared to those imposed by triblock copolymers, in which the two chain ends of the PE block are tethered to two glassy blocks (PS, or PS and PMMA), as evidenced by the T_m variations discussed in Figure 1. Therefore, the SN effects of diblock copolymers and triblock co- and terpolymers are discussed separately. For clarity, in this work, once the T_c observed after cooling from different T_s exceeds the standard crystallization temperature by more than 0.5 °C, SN is considered to occur.

Figure 2a,b presents the DSC cooling and subsequent heating curves for the $E_{42}M_{58}$[54] diblock copolymer after SN over a broad range of T_s values. This diblock copolymer exhibits a lamellar morphology in the melt and is strongly segregated, as shown in the cartoon represented in Figure 2d. Hence, the PE block crystallizes within the established lamellar morphology upon cooling from the microphase-segregated melt. The results for neat PE as a reference are presented in Figure S2 (Supporting Information). In our previous report, we proposed that the two crystallization peaks observed in the diblock copolymers correspond to different nucleation mechanisms.[51,55] The primary exotherm at higher temperatures (labeled T_{c2}) is attributed to the crystallization of lamellar PE MDs with heterogeneities, which are interconnected by the typical block copolymer lamellar morphology defects. In contrast, the much smaller crystallization peak (labeled T_{c1}) at lower temperatures probably corresponds to the crystallization of a very small fraction of isolated MDs. For those, nucleation probably occurs by less active heterogeneities or at the MD interphase since T_c is too high to originate from homogeneous nucleation.

Plotting the T_c values against the T_s temperatures superimposed on the "standard" DSC melting curve of the block copolymer helps to better understand the positioning of the different *Domains* relative to the melting of the original crystals. As shown by the variation of the main crystallization peak values (T_{c2}) in Figure 2c, the PE block within $E_{42}M_{58}$[54] exhibits classical SN behavior with three distinct characteristic SN *Domains*, similar to the results for neat PE shown in Figure S2 (Supporting Information).

For $T_s \geq 122$ °C, T_{c2} remains constant, and this temperature is referred to as the standard crystallization temperature. The material is melted into an isotropic melt, corresponding to *Domain I*, where only high-temperature-resistant heterogeneities can act as nuclei to induce crystallization.

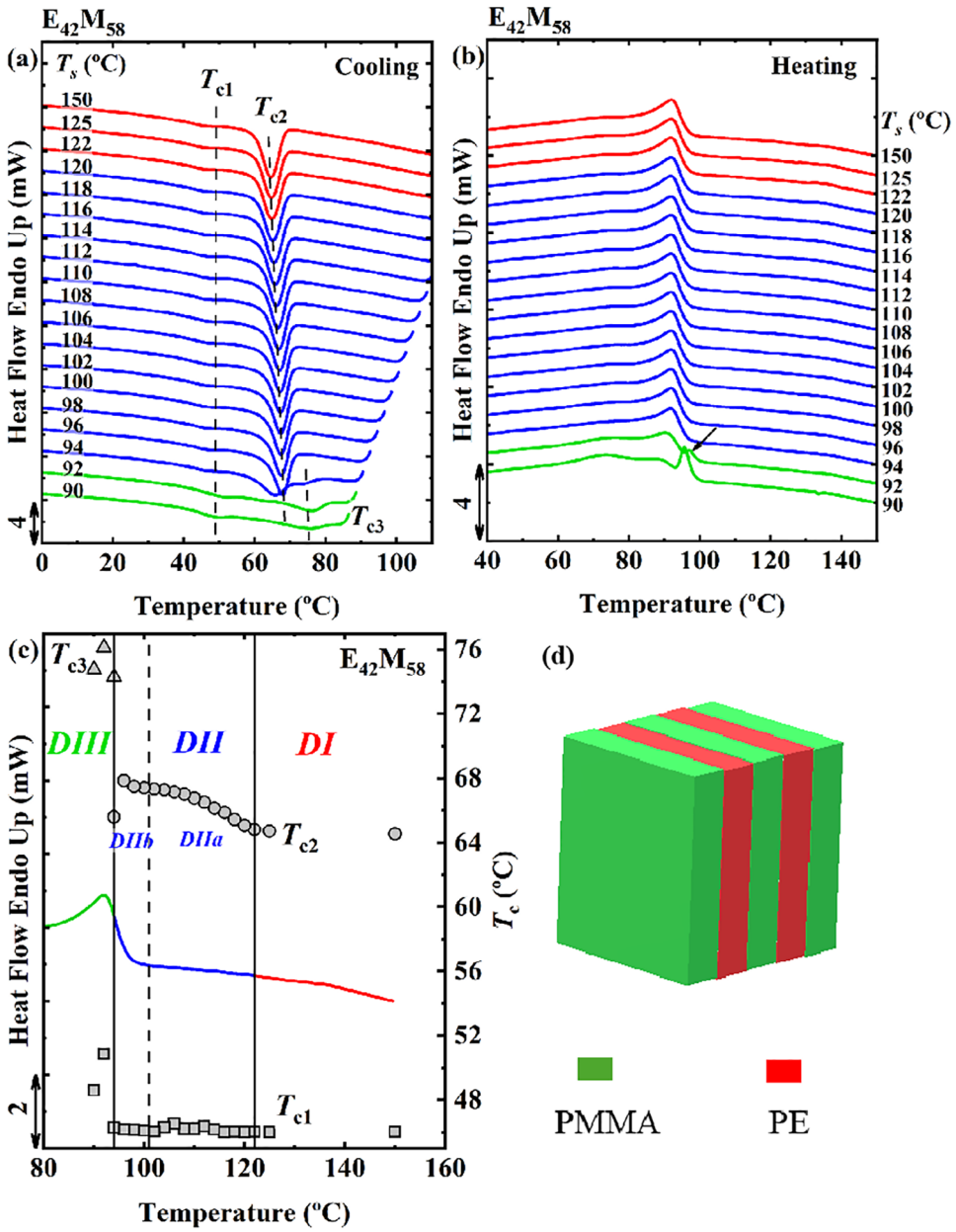

Figure 2. DSC cooling a) and heating b) scans after SN at indicated temperatures (T_s) for $E_{42}M_{58}{}^{54}$. c) SN *Domains* superposed to the DSC melting trace. The solid vertical lines in (c) indicate the transition between the indicated *Domains*, and the vertical dashed line indicates the separation of *Domain II* into *DIIa* and *DIIb*. T_c values are plotted on the right *y*-axis as a function of T_s. The colors of the DSC traces indicate the different SN *Domains*. Red = *Domain I*, blue = *Domain II*, green = *Domain III*. d) Schematic cartoon of the $E_{42}M_{58}{}^{54}$ morphology (alternating PE/PMMA lamellae).

For T_s values between 122 °C > T_s ≥ 94 °C, the PE blocks undergo SN (*Domain II*). In this range, T_{c2} gradually increases as T_s decreases, with its increment relative to the standard crystallization temperature exceeding 0.5 °C, reflecting an acceleration in non-isothermal crystallization kinetics caused by SN. Additionally, no extra thermal signals are observed in the corresponding melting peaks (Figure 2b), indicating that the sample is in *Domain II* (*self-nucleation Domain*) in the temperature range of T_s values where the DSC curves are drawn in blue color in Figure 2. Müller et al.[41,42] proposed that within *Domain II*, the existence of *sub-dDomains DIIa* and *DIIb* can be differentiated with the help of the end of the standard melting endotherm. As the temperature exceeds 101 °C, the DSC baseline levels off, and the DSC cannot record any further latent heat of fusion. This indicates that 101 °C is the end of the melting endotherm for the $E_{42}M_{58}{}^{54}$ diblock copolymer. *DIIa* or the *melt memory Domain* corresponds to the temperature range above 101 °C, where all crystals are molten, leaving no detectable melting transitions by DSC. In this case, the SN observed is due to the melt memory effects. In *DIIb* or the *self-seeding Domain*, small crystal fragments that do not undergo annealing remain in the melt and can act as self-seeds to induce SN.

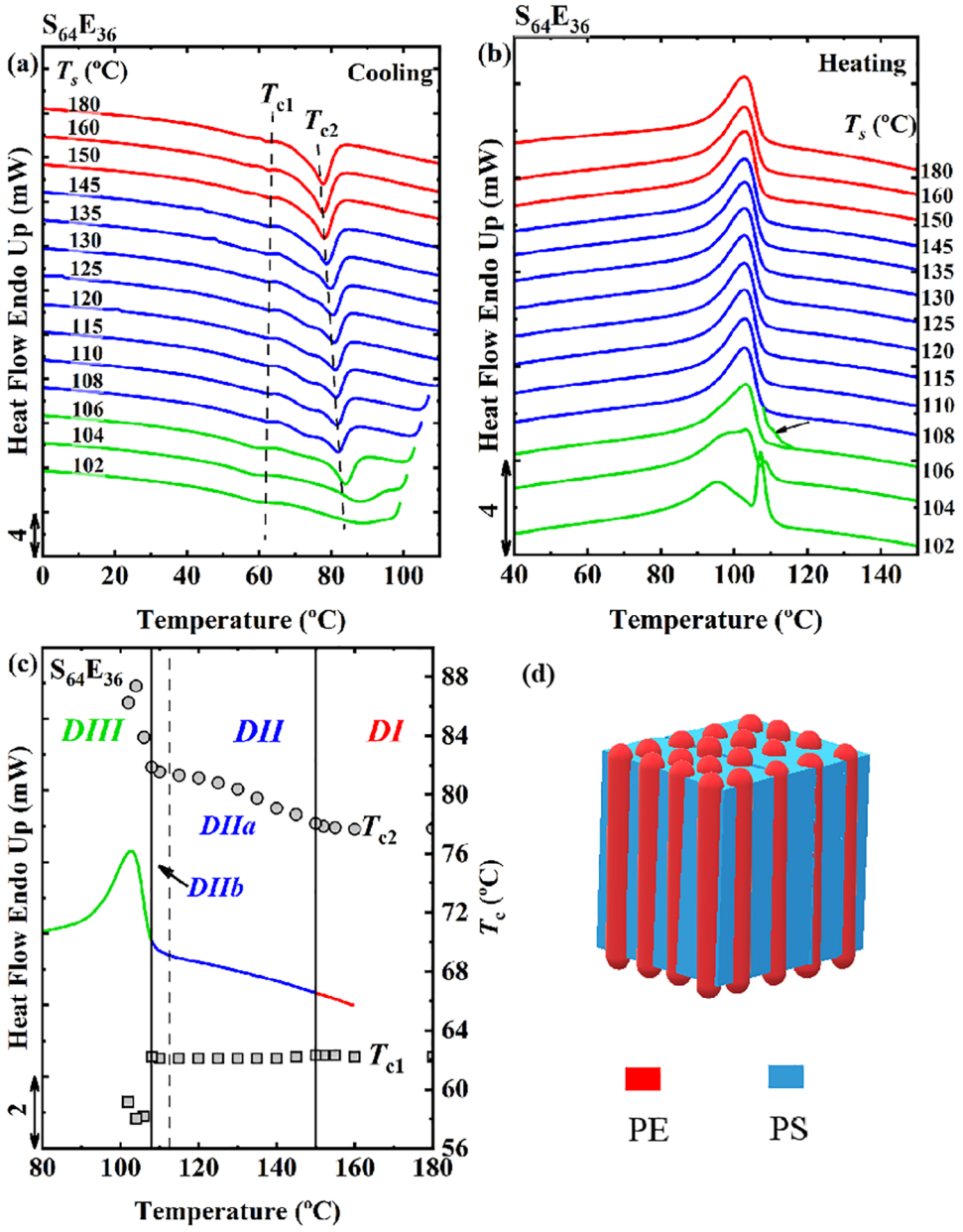

Figure 3. a) DSC cooling and b) heating scans after SN at indicated temperatures (T_s) for the $S_{64}E_{36}{}^{74}$ diblock copolymer. c) SN *Domains* superposed to the DSC melting trace. d) Schematic cartoon of the $S_{64}E_{36}{}^{74}$ morphology (PE cylinders in PS matrix).

The appearance of an endothermic peak at the tail of the melting endotherm for $T_s \leq 92$ °C (indicated by an arrow in Figure 2b) identifies the boundary of traditional *Domain III* ($DIII_{SA}$). In this *Domain*, unmelted crystal fragments undergo SN and annealing during thermal conditioning at the T_s for 5 min, increasing their melting point.

The plot of T_{c1} versus T_s for the PE fraction crystallizing in the low-temperature exotherm in Figure 2c shows no significant change for $T_s \geq 94$ °C. This observation suggests the absence of *DII* in this case, as there is no shift in T_c to higher temperatures with decreasing T_s. However, in $DIII_{SA}$ as defined by the change in T_{c2}, the value of T_{c1} also shows a slight increase, indicating the onset of SN. Thus, for the small fraction of PE blocks crystallizing in isolated MDs, while no traditional *DII* is present, SN can still be induced by self-seeds within *DIII*. It is noted that a very small exothermic peak at a relatively high temperature labeled T_{c3} is found as the T_s decreases to 94 °C. This may be attributed to the crystallization of different segments of the PE block. Because of restricted diffusion, the segments near the PMMA domain interface may encounter more significant difficulties in SN and can only start to self-nucleate at a lower T_s.

Similar to $E_{42}M_{58}{}^{54}$, classical SN behavior was obtained for the $S_{64}E_{36}{}^{74}$ diblock copolymer (**Figure 3**). The $S_{64}E_{36}{}^{74}$ diblock copolymer forms PE cylinders embedded in a PS matrix because of its lower PE content, as shown in Figure 3d. Hence, the tiny exothermic peak at a lower temperature (T_{c1}) corresponds

to the crystallization of a small amount of isolated PE cylinders (Figure 3a). Therefore, the occurrence of SN is primarily reflected by the shift of the main crystallization peak at T_{c2}, where percolated PE cylinders crystallize nucleated by the existing heterogeneities. Starting from high temperatures and moving downward, the increase in the main crystallization peak temperature (T_{c2}) for T_s < 150 °C indicates the presence of *DII*. When T_s drops to 106 °C, the *Domain* III_{SA} is defined by the continuous increase in T_{c2} values accompanied by the emergence of a high-temperature shoulder on the corresponding melting endotherm (indicated by an arrow in Figure 3b), where annealed crystals (during the 5 min at T_s) melt.

In the case of the small crystallization exotherm of the isolated PE cylinders at T_{c1} *Domain II* is absent. However, T_{c1} exhibits a decrease rather than an increase within *DIII*, which indicates that only annealing occurs without SN, corresponding to *Domain* III_A ($DIII_A$). This is different from the crystallization of the isolated lamellar PE MDs in $E_{42}M_{58}{}^{54}$. Although the boundary temperatures between *DI*/*DII* and *DII*/*DIII* for the $S_{64}E_{36}{}^{74}$ diblock copolymers are higher (due to the lower amount of 1,2-PB units, see Table 1) than those for $E_{42}M_{58}{}^{54}$, a direct transition from *DI* to $DIII_A$ for the crystallization of isolated PE cylinders suggests that SN is more challenging than in the isolated PE lamellae within $E_{42}M_{58}{}^{54}$. This difficulty arises because the injection of self-nuclei into each MD is more constrained, given the larger number of MDs in $S_{64}E_{36}{}^{74}$.

3.3. SN Behavior in Triblock Co- and Terpolymers

For block copolymers, it has been found that the number of free ends of the crystallizable block has a marked influence on crystallization.[3,38,49] Compared to diblock copolymers, the PE middle block in the studied triblock co- and terpolymers is covalently bound at both ends to other blocks that impose stronger constraints for the crystallization of the PE block. As a result, their crystallization behavior and morphology are influenced by the PE block content and the type and length of the other blocks.[51] Considering that the triblock co- and terpolymers under investigation include cases with one or two crystallizable blocks and variations in block symmetry, we will discuss these scenarios separately in the following sections.

3.3.1. PS-b-PE-b-PS Triblock Copolymer with a Single Crystallizable Block

The symmetric triblock copolymer $S_{38}E_{23}S_{39}{}^{105}$ comprises a crystallizable PE middle block covalently linked to two PS blocks of equal length and exhibits a cylindrical morphology with isolated PE cylinders (an inevitable fact given the double tethering of the PE chain ends) embedded within a PS matrix (**Figure 4d**). In Figure 4a, the curves in *Domain I* (red DSC traces) show that the T_c of the isolated PE cylinders is ≈55 °C, a temperature much lower than that of neat PE (≈84 °C). This attests to the isolated character of the cylinders, which do not crystallize at the bulk material's typical heterogeneously induced nucleation temperature. As the PE block is confined to isolated cylinders, the number of cylindrical MDs is much higher (≈10^{15} cylinders cm^{-3}) than the amount of highly active heterogeneities in the bulk material (≈10^9 heterogeneities cm^{-3}).[4,11] Therefore, the cylinders can be considered statistically clean, and the PE block chains either nucleate at the MD surface or homogeneously. Previous literature has proven that PE tends to nucleate at the surface of cylindrical MDs or at the interphase in block copolymers rather than inside the volume of the cylinders (which would correspond to homogeneous nucleation).[4,11]

This $S_{38}E_{23}S_{39}{}^{105}$ triblock copolymer displays an atypical SN behavior, as illustrated in Figure 4. For $T_s \geq 92$ °C, the crystallization peak at T_{c1} remains nearly unchanged, independent of the value of T_s. However, when T_s decreases to 90 °C, the crystallization peak unexpectedly shifts to lower temperatures, contrary to the expected trend. Meanwhile, a weak endothermic peak appears at the high-temperature shoulder of the melting peak during the subsequent heating process (indicated by an arrow in Figure 4b), suggesting the occurrence of crystal fragments annealing.

These observations allow the delineation of SN *Domains*, as depicted in Figure 4c. A direct transition from *DI* to $DIII_A$ deviates from the classical behavior established by Fillon et al.[36] T_c does not increase within the tested T_s temperature range, indicating the absence of a *self-nucleation Domain* (*DII*). Within *DIII*, T_{c1} exhibits a counterintuitive decreasing trend, suggesting that only annealing occurs without SN, corresponding to the previously defined $DIII_A$. However, a small population of crystals can be self-nucleated in the defined $DIII_A$, which is indicated in Figure 4a as T_{c2}. This is similar to the behavior observed for $E_{42}M_{58}{}^{54}$ (Figure 2) and probably corresponds to the crystallization of segments near the PS domain interface. These may encounter more significant difficulties in SN due to limited diffusion and can only start to self-nucleate at a lower T_s. More research would be needed to ascertain the exact reason for this behavior.

As reported previously, the diblock copolymer $S_{64}E_{36}{}^{74}$ and the triblock copolymer $S_{38}E_{23}S_{39}{}^{105}$ exhibit the same morphology (PE cylinders in PS matrix, see Table 1 and Figures 3d and 4d).[51] Although the main exothermic peak of the diblock copolymer exhibits classical SN behavior with the traditional three *Domains*, the tiny peak at lower temperatures, corresponding to the crystallization of isolated MDs, presents a similar trend to that observed in the triblock copolymer with decreasing T_c in *DIII*. Therefore, the disappearance of *DII* and the definition of $DIII_A$ in the $S_{38}E_{23}S_{39}{}^{105}$ triblock copolymer can be explained from two perspectives. On the one hand, the triblock copolymer contains a lower proportion of the crystallizable PE block, enabling the formation of isolated MDs embedded in the vitrified PS matrix, exceeding the number of self-nuclei. On the other hand, the PE blocks are covalently linked at both ends to the PS blocks, creating stronger topological constraints. The pronounced confinement effect inhibits the movement of macromolecular chains, thereby retarding the crystal growth from the nucleus. These observations demonstrate that even block copolymers with identical morphologies can exhibit drastically different SN behavior determined by different chain tethering and, hence, confinement.

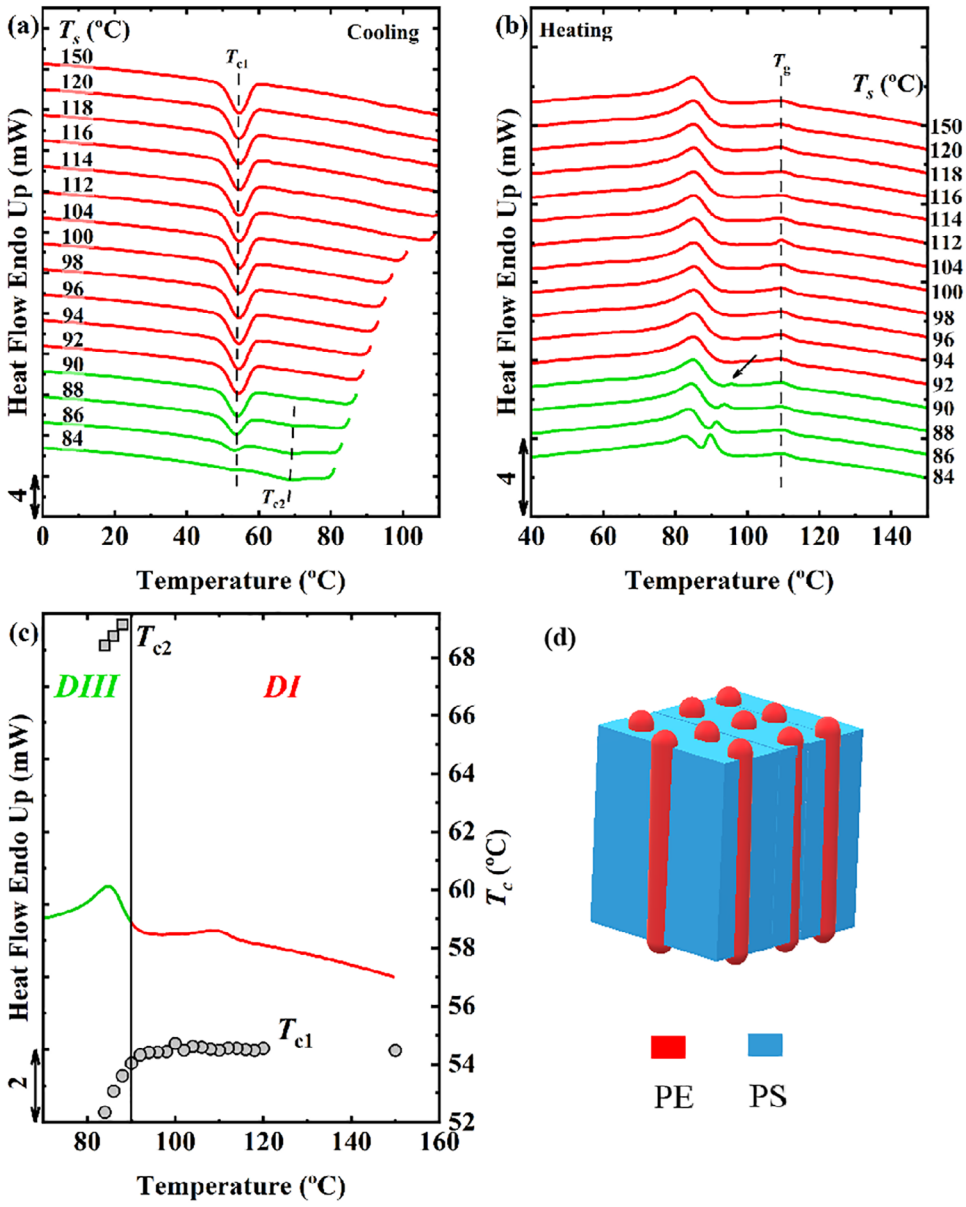

Figure 4. a) DSC cooling and b) heating scans after SN at indicated temperatures (T_s) for the symmetric ABA triblock copolymer $S_{38}E_{23}S_{39}^{105}$. c) SN *Domains* superposed to the DSC melting trace of $S_{38}E_{23}S_{39}^{105}$. T_c values are plotted on the right *y*-axis as a function of T_s (reported on the *x*-axis). The weak transition at ≈110 °C in (b) corresponds to the T_g of the PS matrix. d) Schematic cartoon of the $S_{38}E_{23}S_{39}^{105}$ morphology (PE cylinders in PS matrix).

3.3.2. PS-b-PE-b-PMMA Triblock Terpolymers with a Single Crystallizable Block

Moving to PS-*b*-PE-*b*-PMMA (SEM) triblock terpolymers (**Figure 5**), where the PE block is tethered between two different glassy blocks (PS and PMMA), a similar SN behavior to that found in the symmetric SES triblock copolymer (see Figure 4) can be observed. Regardless of the composition, i.e., formed morphology (Scheme 1 and Figure 5d), all three SEM triblock terpolymers exhibit a direct transition from *DI* to *DIII* (including $DIII_{SA}$ and $DIII_A$) with the absence of *DII*. Interestingly, for $S_{31}E_{36}M_{33}^{96}$, which has the highest PE content among the three samples and exhibits a lamellar morphology with PE lamellae sandwiched between PS and PMMA lamellae (Figure 5d), a slight increase in T_c for the dominant exotherm (i.e., T_{c2}) is observed within *DIII* as T_s decreases. In this *Domain*, crystal annealing has already taken place and, hence, indicates that SN and annealing occur simultaneously. Therefore, *DIII* of this sample can be classified as $DIII_{SA}$. In contrast, for the other two samples with increasingly lower PE content ($S_{23}E_{26}M_{51}^{148}$ and $S_{40}E_{21}M_{39}^{108}$), their T_c values within *DIII* consistently show a decreasing trend rather than an increase. This indicates that SN does not occur and only crystal annealing takes place. Therefore, *DIII* for these samples is classified as $DIII_A$.

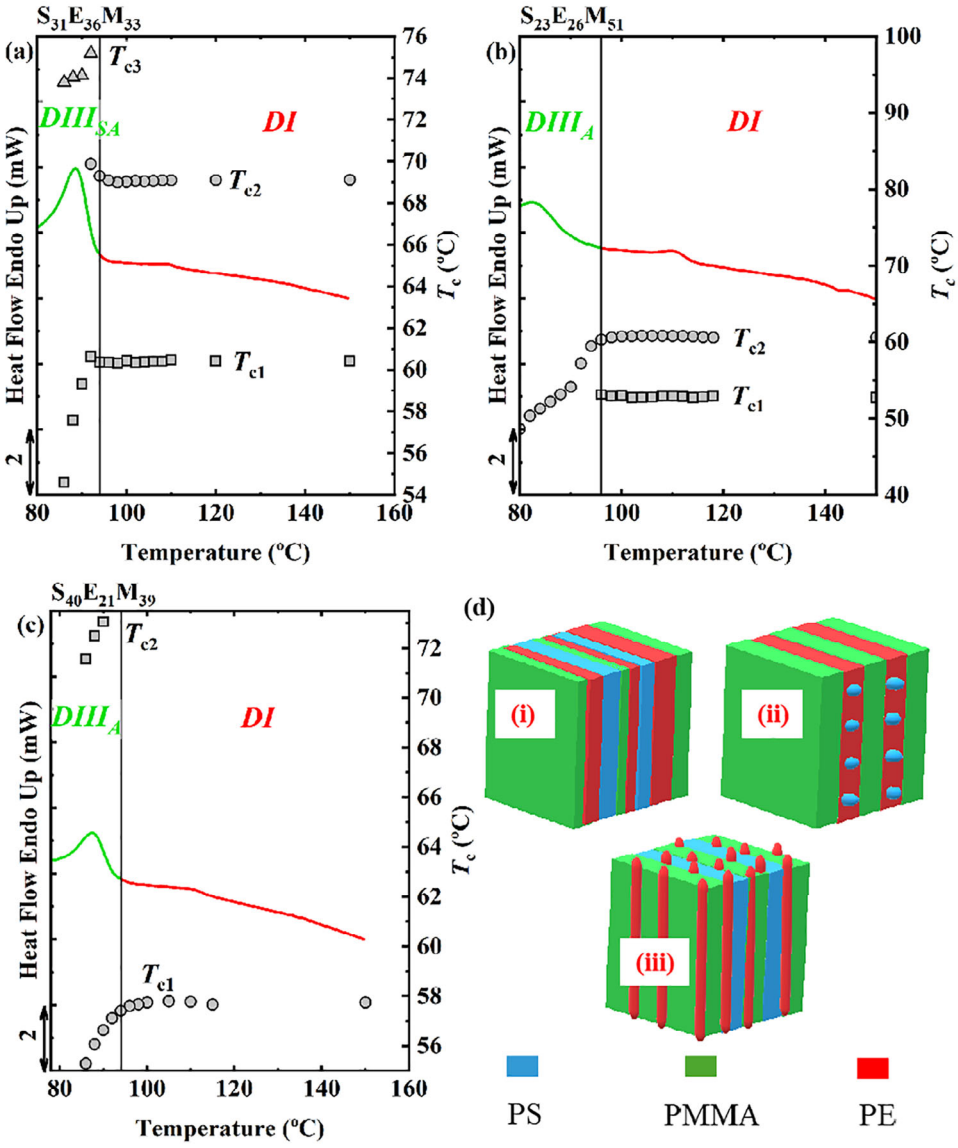

Figure 5. SN *Domains* superposed to their DSC melting trace for a) $S_{31}E_{36}M_{33}{}^{96}$, b) $S_{23}E_{26}M_{51}{}^{148}$, and c) $S_{40}E_{21}M_{39}{}^{108}$. T_c values are plotted on the right *y*-axis as a function of T_s (reported on the *x*-axis). Respective cooling and heating traces after SN are given in Figures S3–S5 (Supporting Information). d) Schematic cartoons of BCP morphologies: (i) PE lamellae sandwiched between PS and PMMA lamellae for $S_{31}E_{36}M_{33}{}^{96}$, (ii) PS cylinders in PE lamellae + PMMA lamellae for $S_{23}E_{26}M_{51}{}^{148}$, and (iii) PE cylinders sandwiched between PS and PMMA lamellae for $S_{40}E_{21}M_{39}{}^{108}$.

For the symmetric SEM triblock copolymers, a new exothermic peak was observed at higher temperatures in *DIII* (*DIII*$_{SA}$ for $S_{31}E_{36}M_{33}{}^{96}$ and DIIIA for $S_{40}E_{21}M_{39}{}^{108}$), as shown in Figures S3 and S5 (Supporting Information). This phenomenon is similar to that observed in $E_{42}M_{58}{}^{54}$ and $S_{38}E_{23}S_{39}{}^{105}$ block copolymers and may be attributed to the restricted chain mobility near the glassy phase interfaces during crystallization. Such a restriction makes it more difficult for SN to occur in the segments, resulting in SN being triggered only at lower T_s.

Comparing the behavior of the three SEM samples, the molecular constraints imposed by the glassy matrix are similar despite the differences in PS and PMMA block lengths. However, it appears that the ability to undergo self-nucleation (even within *DIII*) is correlated with the PE content.[31] On the other hand, the final morphology of the block copolymer determines the degree of confinement of the PE blocks, which influences SN. Although the crystallizable PE blocks in both $S_{31}E_{36}M_{33}{}^{96}$ and $S_{23}E_{26}M_{51}{}^{148}$ generate lamellar structures, the extent of confinement differs significantly between the two. In $S_{31}E_{36}M_{33}{}^{96}$ the PE lamellae are sandwiched between PS and PMMA lamellae, resulting in a relatively weaker confinement on the crystallization. In contrast, while $S_{23}E_{26}M_{51}{}^{148}$ also forms alternating PE and PMMA lamellae, the PE lamellae are disrupted by embedded PS cylinders, creating more confined regions and preventing SN. For $S_{40}E_{21}M_{39}{}^{108}$ the PE blocks form cylindrical domains tightly sandwiched between PS and PMMA lamellae, leading to even stronger confinement effects on the crystallization process. In summary, the results obtained by comparing these three SEM samples show that

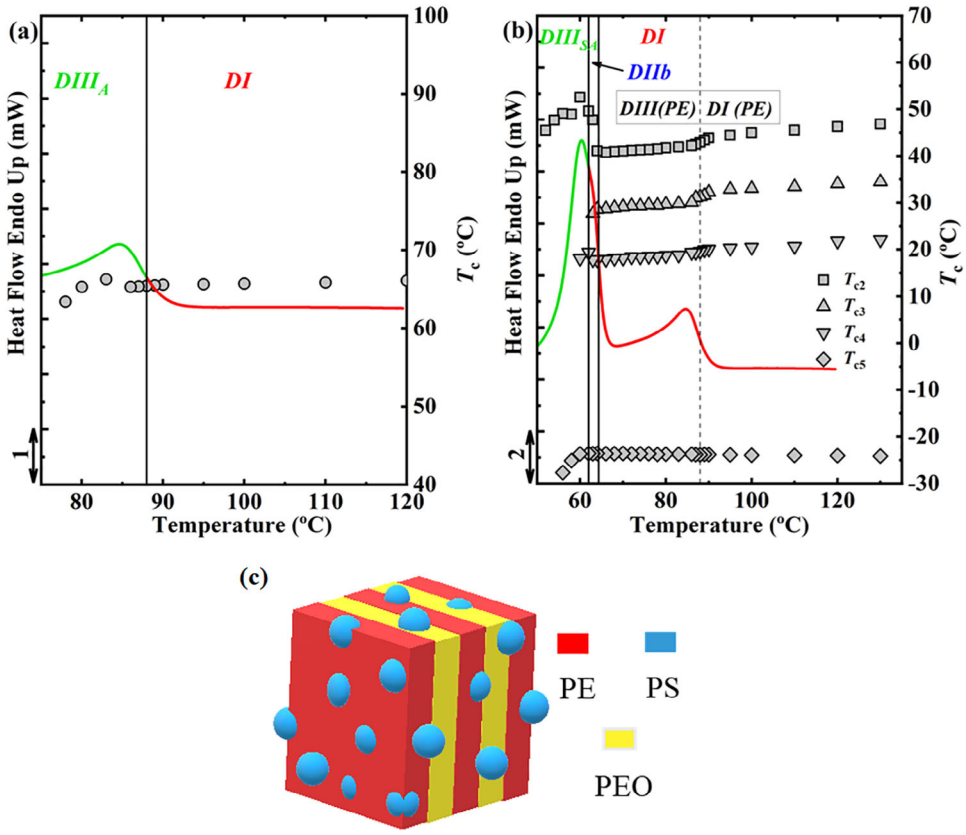

Figure 6. SN *Domains* for the a) PE block and b) PEO block in $S_{31}E_{38}EO_{31}{}^{92}$ superposed to the DSC melting trace. The dashed line in (b) indicates the boundary between *DI* and $DIII_A$ for the PE block. c) Schematic cartoon of the $S_{31}E_{38}EO_{31}{}^{92}$ morphology (distorted PS domains in PE lamellae + PEO lamellae).

they all possess a high enough confinement to lack *DII*. However, as the degree of confinement in the triblock terpolymers increases, *DIII* switches from the classical *DIII* (i.e., $DIII_{SA}$) to $DIII_A$.

3.3.3. PS-*b*-PE-*b*-PEO Triblock Terpolymer with Two Crystallizable Blocks

When a system is composed of two or more crystallizable components, it becomes intriguing to explore how the crystallization of one block influences the other.[9–11] For instance, the crystallization of one component might either promote or hinder the crystallization of the other, depending on the interactions and confinement effects within the system.[15,37,49,56,57] In the case of PS-*b*-PE-*b*-PCL triblock terpolymers, it has been reported that the PE block does not exhibit a nucleation effect on the crystallization of PCL. On the contrary, an antinucleation effect was observed.[37,49] The SN behavior of PS-*b*-PE-*b*-PCL strongly depends on the PE content. When the PE content is as low as 15 wt.%, *DII* disappears and annealing occurs before SN.

The $S_{31}E_{38}EO_{31}{}^{92}$ triblock terpolymer exhibits a very complex morphology (see Table 1), where the PE and PEO blocks form alternating lamellae, similar to $S_{23}E_{26}M_{51}{}^{148}$, but with PS domains irregularly embedded within the PE lamellae.[51] Therefore, SN experiments were performed to resolve the influence of this complex morphology on the confinement acting on the crystallizable PE and PEO blocks.

Figure S6 (Supporting Information) presents the cooling and subsequent heating DSC scans after SN at the indicated T_s values. The crystallization peak at the highest temperature (T_{c1}) corresponds to the crystallization of the PE block. On the other hand, the remaining exothermic peaks at lower temperatures ($T_{c2} - T_{c5}$) are attributed to the fractionated crystallization of PEO.[55] During the melting process, the two endothermic peaks at high and low temperatures correspond to the melting of PE and PEO crystals, respectively. Given the presence of two crystallizable blocks, we will discuss the SN *Domains* of PE and PEO separately.

As shown in **Figure 6a**, a non-classical SN behavior was observed for the PE block. The T_c of the PE block remains constant within *DI* until it shows a decreasing trend in *DIII*, indicating the absence of *DII* and that only annealing occurs in *DIII* without SN. Therefore, a direct transition from *DI* to $DIII_A$ can be observed for the PE block in the $S_{31}E_{38}EO_{31}{}^{92}$ triblock terpolymer. It should be noted that this is similar to the behavior of the PE block within $S_{40}E_{21}M_{39}{}^{108}$ and $S_{23}E_{26}M_{51}{}^{148}$.

In the case of the PEO block, fractionated crystallization occurs.[17,51,55] The first crystallization peak at T_{c2} is attributed to heterogeneously nucleated PEO lamellae, while the lowest temperature crystallization peak at T_{c5} results from homogeneous nucleation within isolated PEO microdomains.[55] The intermediate peaks (T_{c3} and T_{c4}) can be assigned to crystallization af-

ter nucleation by less active heterogeneities and interfacial nucleation of a small fraction of PEO lamellae.[51] As shown in Figure 6b, SN can occur for the heterogeneously nucleated PEO MDs, as the crystallization temperature T_{c2} increases with decreasing T_s. This corresponds to residual crystals acting as self-seeds, thus establishing *DIIb* before entering *DIII*. While classic SN behavior can be observed for these heterogeneously nucleated PEO MDs, the extremely narrow *DII* and the absence of the *melt memory Domain* (*DIIa*) suggest that the SN effect is significantly suppressed compared to PEO homopolymers (Figure S2, Supporting Information). It is also noteworthy that T_{c3} and T_{c4} vanish upon entry into $DIII_{SA}$ for the heterogeneously nucleated PEO MDs.

In addition, for the homogeneously nucleated isolated PEO MDs at T_{c5}, the *self-nucleation Domain* is absent, as expected.[4,11] The pronounced decrease in T_{c5} within *DIII* confirms a direct transition from *DI* to $DIII_A$. This decrease may result from the antinucleation effect induced by the earlier crystallization of PE crystals.[37]

3.4. Comparison of SN Behavior of the PE Blocks in Di- and Triblock Copolymers

As discussed above, factors such as the final morphology and confinement in block copolymers significantly influence the SN behavior of the PE block. However, the exact role of PE content in these phenomena remains unclear. The widths of the *self-nucleation Domains* (*DII*, *DIIa*, and *DIIb*) are plotted as a function of PE content in **Figure 7**. The neat PE obtained through the hydrogenation of PB (89 mol% 1,4-units) as well as the PE blocks within the block copolymers, exhibit a branched structure (Table 1), which induces a significant melt memory effect.[58,59]

Interestingly, as the PE content decreases, the diblock copolymers $E_{42}M_{58}{}^{54}$ and $S_{64}E_{36}{}^{74}$ show even stronger melt memory effects as evidenced by the wider *DIIa*, with the latter displaying a much broader *DIIa* than the former. This unexpected phenomenon suggests that the reduction in PE content combined with the confinement effect inherent to block copolymers enhances rather than diminishes the melt memory. The molecular weight of the PE blocks is within the range of 23–27 kg mol^{-1} for both diblock copolymers and, hence, should not play a decisive role. Accordingly, this behavior is likely closely related to their different morphology. In the diblock copolymers, the T_g values of PS and PMMA are higher than T_c and T_m of PE. As a result, during both the SN and crystallization processes upon cooling, the molecular motion of PE chains is constrained within cylindrical or lamellar domains embedded in a vitreous matrix. Upon cooling from the melt, the selection process of crystallizable chains (which occurs due to molecular segregation during crystallization) reduces the nucleation barrier for subsequent crystallization, increasing the crystallization temperature. Moreover, the constraints on molecular chain diffusion in the melt are stronger in PE cylinders than in lamellae, which increases the temperature required to reach an isotropic melt. Hence, the $S_{64}E_{36}{}^{74}$ diblock copolymer exhibits a more pronounced melt memory effect.[26] The topological constraints preserve part of the original conformation that the chains had in the crystal lattice, enhancing melt memory. However, this effect is only present in the diblock copolymers in Figure 7. A possible explanation is that confinement can trigger melt memory in diblock copolymers. However, the melt memory disappears when the confinement degree is too high, as in the case of the triblock co- and terpolymers. Consequently, our results indicate that the melt memory of the PE block goes through a maximum as the confinement degree increases.

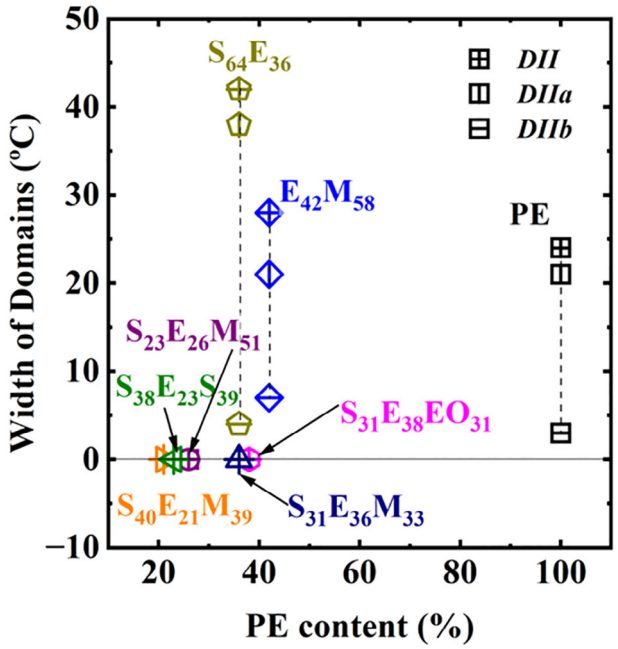

Figure 7. Width of *DII*, *DIIa*, and *DIIb* as a function of the PE block content ($E_{42}M_{58}{}^{54}$: alternating PE/PMMA lamellae; $S_{64}E_{36}{}^{74}$ and $S_{38}E_{23}S_{39}{}^{105}$: PE cylinders in PS matrix; $S_{40}E_{21}M_{39}{}^{108}$: PE cylinders sandwiched between PS and PMMA lamellae; $S_{31}E_{36}M_{33}{}^{96}$: PE lamellae sandwiched between PS and PMMA lamellae; $S_{23}E_{26}M_{51}{}^{148}$: PS cylinders in PE lamellae + PMMA lamellae; $S_{31}E_{38}EO_{31}{}^{92}$: distorted PS domains in PE lamellae + PEO lamellae).

The SN behavior of all samples has been summarized in **Table 2**, focusing primarily on the presence or absence of each *Domain* and *sub-Domain*, taking into account that SN may also disappear within *DIII* in certain block copolymers. The table is organized in descending order of PE content. The disappearance

Table 2. SN behavior of the PE block in the block copolymers examined in this work.

Sample	*DI*	*DII*		$DIII_{SA}$	$DIII_A$
		DIIa	*DIIb*		
PE	✓	✓	✓	✓	✗
$E_{42}M_{58}{}^{54}$	✓	✓	✓	✓	✗
$S_{31}E_{38}EO_{31}{}^{92}$	✓	✗	✗	✗	✓
$S_{64}E_{36}{}^{74}$	✓	✓	✓	✓	✗
$S_{31}E_{36}M_{33}{}^{96}$	✓	✗	✗	✓	✗
$S_{23}E_{26}M_{51}{}^{148}$	✓	✗	✗	✗	✓
$S_{38}E_{23}S_{39}{}^{105}$	✓	✗	✗	✗	✓
$S_{40}E_{21}M_{39}{}^{108}$	✓	✗	✗	✗	✓

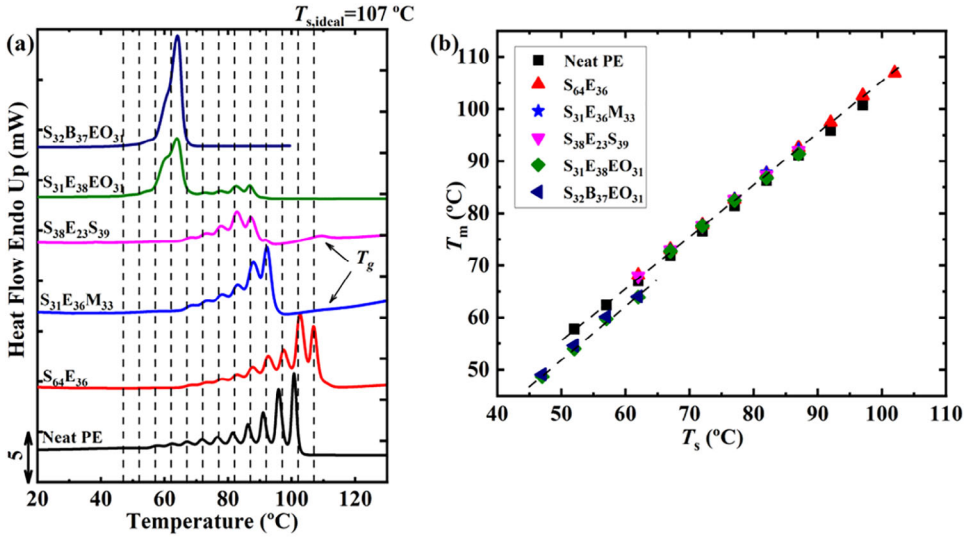

Figure 8. a) Final heating scans at 20 °C min^{-1} after SSA thermal treatments using the same ideal self-nucleation temperature $T_{s,ideal}$ = 107 °C for all block copolymers and neat PE. The fractionation window was 5 °C. b) Peak T_m values of each thermal fraction created by SSA treatments as a function of T_s. BCP morphologies: $S_{64}E_{36}$[74] and $S_{38}E_{23}S_{39}$[105]: PE cylinders in PS matrix; $S_{31}E_{36}M_{33}$[96]: PE lamellae sandwiched between PS and PMMA lamellae; $S_{31}E_{38}EO_{31}$[92]: distorted PS domains in PE lamellae + PEO lamellae; $S_{32}B_{37}EO_{31}$[91]: PB lamellae sandwiched between PS and PEO lamellae.

of *DII* (*DIIa* and *DIIb*) is a universal feature of all triblock co- and terpolymers independent of the PE content in a composition range where PE is always the minority component (i.e., in the present work, the PE content is in the range of 21–38 wt.%). The $S_{31}E_{36}M_{33}$[96] triblock terpolymer exhibits not only annealing but also SN in *DIII*. However, SN within *DIII* disappears with decreasing PE content or in the presence of a second crystallizable block (i.e., for $S_{31}E_{38}EO_{31}$[92]), leaving annealing as the sole process.

Although both the $S_{38}E_{23}S_{39}$[105] triblock copolymer and the $S_{64}E_{36}$[74] diblock copolymer exhibit a similar cylindrical morphology, the lower PE content and the constraint at both ends of the PE block in the triblock copolymer prevent the activation of sufficient effective self-nuclei. A striking comparison can be drawn between $S_{64}E_{36}$[74] and $S_{31}E_{36}M_{33}$[96]. Despite having identical crystallizable block contents, the morphology and confinement effects in the triblock terpolymer play a decisive role in suppressing SN. Overall, the decrease in PE content and the increase in confinement result in the disappearance of SN, starting in *DII* and extending into *DIII*.

3.5. SSA Studies

The SSA technique is fundamentally a thermal fractionation method that relies on sequentially applying SN and annealing cycles to a polymer material.[44,46,52–54] Following the thermal protocol described in Scheme 2b, the final DSC heating scan reveals a distribution of a series of melting peaks as a result of the SSA treatment, as shown for representative samples in **Figure** 8a. For comparison purposes, a maximum ideal self-nucleation temperature of $T_{s,ideal}$ = 107 °C was applied to all samples with a fractionation window of 5 °C.

Figure 8b displays the peak T_m values of the fractions plotted against the respective employed T_s. The plot shows two distinct linear relationships, each corresponding to the crystalline fractions of the PE and PEO blocks, respectively, indicating the correct application of the SSA thermal protocol.[44]

The fractionated neat PE (hydrogenated PB with 89 mol% 1,4-units) exhibits a series of melting peaks, each corresponding to the melting of crystalline fractions with varying lamellar thicknesses formed and annealed at each T_s below the $T_{s,ideal}$. This is expected, as the molecular structure of hydrogenated PB contains ethyl branches randomly distributed along the chains. Each branch interrupts the linear crystallizable sequences and, thus, facilitates the fractionation by the SSA treatment. The random distribution of branches is reflected in the monomodal distribution of the thermal fractions.[44] This observation is consistent with the previously discussed melt memory effect in neat PE.

A similar result was observed for the $S_{64}E_{36}$[74] diblock copolymer, showing a comparable series of unimodally distributed melting peaks (Figure 8a). In contrast to the results for neat PE, the highest melting peak temperature was slightly increased, consistent with the standard DSC test results showing that $S_{64}E_{36}$[74] has fewer branches (see Table 1) and, thus, a higher melting point.

Triblock copolymers with a single semi-crystalline PE block, $S_{31}E_{36}M_{33}$[96] and $S_{38}E_{23}S_{39}$[105], were selected as representative samples. The transition at ≈110 °C corresponds to the T_g of the amorphous blocks. A well-defined series of melting peaks is observed, reflecting the structural defects present in the PE block. However, the lack of high melting fractions, as present in neat PE, reflects that confinement limits the attainable lamellar thicknesses, leading to lower melting point fractions.

A bimodal distribution of melting peaks was observed for the $S_{31}E_{38}EO_{31}$[92] triblock terpolymer, featuring two crystallizable blocks. The distinct series of melting endotherms at higher temperatures corresponds to the PE thermal fractions, while the less-defined melting peaks at lower temperatures represent the PEO fractions. The PEO component is not well fractionated as it is a

linear polymer without branching or any other defects along the chain that can enhance thermal fractionation.[44] As a comparison, the $S_{32}B_{37}EO_{31}^{91}$ triblock terpolymer (the $S_{31}E_{38}EO_{31}^{92}$ precursor) containing only PEO as a crystallizable block exhibited a melting peak distribution similar to the low-temperature part of $S_{31}E_{38}EO_{31}^{92}$ after SSA treatment, confirming the poor fractionation of PEO (Figure 8a).

4. Conclusion

This study investigated the SN behavior of crystallizable blocks within a series of block copolymers with varying architecture (AB diblock copolymers, ABA and ABC triblock co- and terpolymers). In the case of the diblock copolymers PS-*b*-PE and PE-*b*-PMMA, although the glassy amorphous matrix constrains one end of the crystallizable PE block during the crystallization process, a wider *Domain IIa* (*melt memory Domain, DIIa*) than in analogous neat PE is present. This indicates a more pronounced melt memory effect in the diblock copolymers with respect to neat PE, especially when the PE block is confined within cylindrical microdomains. The cylindrical morphology imposes greater topological constraints on the mobility of the confined PE chains, which preserves part of the original conformation that the chains had in the crystals, thus enhancing melt memory. In contrast, when the PE block is tethered on both ends, i.e., for ABA and ABC triblock co- and terpolymers, melt memory was observed to disappear. We speculate that confinement triggers melt memory in diblock copolymers. Still, the melt memory disappears when the confinement degree is too high, as in the case of the triblock co- and terpolymers. Hence, the melt memory of the PE block goes through a maximum as the confinement degree increases.

The *self-nucleation Domain* (i.e., *DII*) in PS-*b*-PE-*b*-PS and PS-*b*-PE-*b*-PMMA triblock co- and terpolymers is absent due to strong confinement, regardless of the PE block content (the PE block was always the confined minority phase with PE fractions ≤ 36 wt.%). The source of this confinement effect is related to the morphology and number of blocks within the material. Although PS-*b*-PE and PS-*b*-PE-*b*-PS share the same morphology (PE cylinders embedded in the PS matrix), the diblock exhibits the strongest melt memory effect observed in this study. In contrast, the PS-*b*-PE-*b*-PS triblock copolymer only displays a direct transition from *DI* (*melting Domain*) to $DIII_A$ (*annealing Domain*) without SN. Similar behavior was observed for a series of PS-*b*-PE-*b*-PMMA triblock terpolymers and a double crystalline PS-*b*-PE-*b*-PEO triblock terpolymer, where the PE blocks are either confined in cylindrical microdomains or form disrupted lamellae. The double tethering of the PE middle block chains enhances the confinement so much that the possibility of SN is virtually eliminated (i.e., absence of *DII* and, in the highest confinement cases, SN disappears even within *DIII*).

All block copolymers exhibit a series of well-defined melting peaks similar to those of neat PE after SSA, confirming the presence of branched structures arising from residual 1,2-units in the respective PB-containing precursors. Although the presence of structural defects has been confirmed, the disappearance of the *self-nucleation Domains* highlights that confinement plays a dominant role in suppressing SN.

Our results show that, next to the block copolymer morphology (determined mainly by composition for sufficiently strong segregation), their architecture (AB-, ABA-, or ABC-type) plays a decisive role in defining the confinement acting on the crystallizable B block. Depending on the confinement strength, melt memory effects can either be enhanced or completely absent, resulting in the disappearance of *self-nucleation Domain II* for strong confinements. This is not only important for the thermal processing of block copolymers with crystallizable blocks but also relevant for baroplastic block copolymers. Tailoring the confinement can help to keep crystallization temperature and degree of crystallinity low enough to achieve baroplastic behavior that is based on the (partial) miscibility of the different blocks when pressure is applied.

Supporting Information

Supporting Information is available from the Wiley Online Library or from the author.

Acknowledgements

The authors acknowledge support from the María de Maeztu Excellence Unit CEX2023-001303-M funded by MCIN/AEI/10.13039/501100011033. This research was also supported by the projects PID2020-113045GB-C21 and PID2023-149734NB-C22 funded by MCIN/AEI/10.13039/501100011033. The authors thank the keylabs "*Synthesis and Molecular Characterization*" and "*Electron and Optical Microscopy*" of the Bavarian Polymer Institute (BPI) at the University of Bayreuth for their support.

Open access funding enabled and organized by Projekt DEAL.

Conflict of Interest

The authors declare no conflict of interest.

Data Availability Statement

The data that support the findings of this study are available in the supplementary material of this article.

Keywords

block copolymers, confinement, crystallizable blocks, self-nucleation, thermal fractionation

Received: January 28, 2025
Revised: April 8, 2025
Published online: May 19, 2025

[1] Y.-L. Loo, R. A. Register, A. J. Ryan, G. T. Dee, *Macromolecules* **2001**, *34*, 8968.
[2] I. W. Hamley, *Adv. Polym. Sci.* **1999**, *148*, 113.
[3] A. J. Müller, V. Balsamo, M. L. Arnal, T. Jakob, H. Schmalz, V. Abetz, *Macromolecules* **2002**, *35*, 3048.
[4] A. J. Müller, V. Balsamo, M. L. Arnal, *Adv. Polym. Sci.* **2005**, *190*, 1.
[5] I. W. Hamley, *The Physics of Block Copolymers*, Oxford University Press, Oxford, **1998**.
[6] I. W. Hamley, *Developments in Block Copolymer Science and Technology*, Wiley, Hoboken, NJ, USA **2004**.

[7] C. Robitaille, J. Prud'homme, *Macromolecules* **1983**, *16*, 665.
[8] P. Rangarajan, R. A. Register, D. H. Adamson, L. J. Fetters, W. Bras, S. Naylor, A. J. Ryan, *Macromolecules* **1995**, *28*, 1422.
[9] A. J. Müller, M. L. Arnal, V. Balsamo, *Progress in Understanding of Polymer Crystallization*, (Eds: G. Reiter, G.R. Strobl), Springer Berlin Heidelberg, Berlin, Heidelberg, **2007**, p. 229.
[10] R. V. Castillo, A. J. Müller, *Prog. Polym. Sci.* **2009**, *34*, 516.
[11] R. M. Michell, A. J. Müller, *Prog. Polym. Sci.* **2016**, *54-55*, 183.
[12] L. Zhu, Y. Chen, A. Zhang, B. H. Calhoun, M. Chun, R. P. Quirk, S. Z. D. Cheng, *Phys. Rev. E* **1999**, *60*, 10022.
[13] L. Zhu, B. R. Mimnaugh, Q. Ge, R. P. Quirk, S. Z. D. Cheng, E. L. Thomas, B. Lotz, B. S. Hsiao, F. Yeh, L. Liu, *Polymer* **2001**, *42*, 9121.
[14] H. Schmalz, A. Knoll, A. J. Müller, V. Abetz, *Macromolecules* **2002**, *35*, 10004.
[15] H. Schmalz, A. J. Müller, V. Abetz, *Macromol. Chem. Phys.* **2003**, *204*, 111.
[16] A. J. Ryan, I. W. Hamley, W. Bras, F. S. Bates, *Macromolecules* **1995**, *28*, 3860.
[17] R. V. Castillo, M. L. Arnal, A. J. Müller, I. W. Hamley, V. Castelletto, H. Schmalz, V. Abetz, *Macromolecules* **2008**, *41*, 879.
[18] Y.-L. Loo, R. A. Register, *Phys. Rev. Lett.* **2000**, *84*, 4120.
[19] V. Balsamo, N. Urdaneta, L. Pérez, P. Carrizales, V. Abetz, A. J. Müller, *Eur. Polym. J.* **2004**, *40*, 1033.
[20] L. Zhu, S. Z. D. Cheng, B. H. Calhoun, Q. Ge, R. P. Quirk, E. L. Thomas, B. S. Hsiao, F. Yeh, B. Lotz, *J. Am. Chem. Soc.* **2000**, *122*, 5957.
[21] S. Nojima, H. Kakihira, S. Tanimoto, H. Nakatani, S. Sasaki, *Polym. J.* **2000**, *32*, 75.
[22] D. J. Quiram, R. A. Register, G. R. Marchand, D. H. Adamson, *Macromolecules* **1998**, *31*, 4891.
[23] J.-T. Xu, S. C. Turner, J. P. A. Fairclough, S.-M. Mai, A. J. Ryan, C. Chaibundit, C. Booth, *Macromolecules* **2002**, *35*, 3614.
[24] H.-L. Chen, J.-C. Wu, T.-L. Lin, J. S. Lin, *Macromolecules* **2001**, *34*, 6936.
[25] D. J. Quiram, R. A. Register, G. R. Marchand, A. J. Ryan, *Macromolecules* **1997**, *30*, 8338.
[26] A. T. Lorenzo, M. L. Arnal, A. J. Müller, A. Boschetti de Fierro, V. Abetz, *Eur. Polym. J.* **2006**, *42*, 516.
[27] A. T. Lorenzo, M. L. Arnal, A. J. Müller, A. Boschetti-de-Fierro, V. Abetz, *Macromolecules* **2007**, *40*, 5023.
[28] A. J. Müller, A. T. Lorenzo, R. V. Castillo, M. L. Arnal, A. Boschetti-de-Fierro, V. Abetz, *Macromol. Symp.* **2006**, *245–246*, 154.
[29] P. Rangarajan, R. A. Register, L. J. Fetters, *Macromolecules* **1993**, *26*, 4640.
[30] M. Mitani, J.-i. Mohri, Y. Yoshida, J. Saito, S. Ishii, K. Tsuru, S. Matsui, R. Furuyama, T. Nakano, H. Tanaka, S.-i. Kojoh, T. Matsugi, N. Kashiwa, T. Fujita, *J. Am. Chem. Soc.* **2002**, *124*, 3327.
[31] G. W. Coates, P. D. Hustad, S. Reinartz, *Angew. Chem., Int. Ed.* **2002**, *41*, 2236.
[32] G. J. Domski, J. M. Rose, G. W. Coates, A. D. Bolig, M. Brookhart, *Prog. Polym. Sci.* **2007**, *32*, 30.
[33] C. De Rosa, R. Di Girolamo, A. Malafronte, M. Scoti, G. Talarico, F. Auriemma, O. Ruiz de Ballesteros, *Polymer* **2020**, *196*, 122423.
[34] C. De Rosa, A. Malafronte, R. Di Girolamo, F. Auriemma, M. Scoti, O. Ruiz de Ballesteros, G. W. Coates, *Macromolecules* **2020**, *53*, 10234.
[35] C. De Rosa, R. Di Girolamo, F. Auriemma, M. D'Avino, G. Talarico, C. Cioce, M. Scoti, G. W. Coates, B. Lotz, *Macromolecules* **2016**, *49*, 5576.
[36] B. Fillon, J. C. Wittmann, B. Lotz, A. Thierry, *J. Polym. Sci., Part B: Polym. Phys.* **1993**, *31*, 1383.
[37] V. Balsamo, A. J. Müller, R. Stadler, *Macromolecules* **1998**, *32*, 7756.
[38] V. Balsamo, Y. Paolini, G. Ronca, A. J. Müller, *Macromol. Chem. Phys.* **2000**, *201*, 2711.
[39] M. L. Arnal, F. López-Carrasquero, E. Laredo, A. J. Müller, *Eur. Polym. J.* **2004**, *40*, 1461.
[40] L. Sangroniz, A. Sangroniz, L. Meabe, A. Basterretxea, H. Sardon, D. Cavallo, A. J. Müller, *Macromolecules* **2020**, *53*, 4874.
[41] R. M. Michell, A. Mugica, M. Zubitur, A. J. Müller, *Adv. Polym. Sci.* **2017**, *276*, 215.
[42] L. Sangroniz, D. Cavallo, A. J. Müller, *Macromolecules* **2020**, *53*, 4581.
[43] Y. Liao, L. Pan, Z. Ma, D. Cavallo, G. Liu, D. Wang, A. J. Müller, *Polymer* **2023**, *282*, 126184.
[44] A. J. Müller, R. M. Michell, R. A. Pérez, A. T. Lorenzo, *Eur. Polym. J.* **2015**, *65*, 132.
[45] D. Zhang, R.-J. Zhao, G.-Q. Ma, Z. Ma, *Chin. J. Polym. Sci.* **2023**, *41*, 1912.
[46] R. A. Pérez-Camargo, D. Cavallo, A. J. Müller, *Front. Soft. Matter* **2022**, *2*, 1003500.
[47] A. J. Müller, J. Albuerne, L. Marquez, J. M. Raquez, P. Degee, P. Dubois, J. Hobbs, I. W. Hamley, *Faraday Discuss.* **2005**, *128*, 231.
[48] A. J. Müller, M. L. Arnal, F. López-Carrasquero, *Macromol. Symp.* **2002**, *183*, 199.
[49] V. Balsamo, A. J. Müller, F. von Gyldenfeldt, R. Stadler, *Macromol. Chem. Phys.* **1998**, *199*, 1063.
[50] M. Wang, J. Li, G. Shi, G. Liu, A. J. Müller, D. Wang, *Macromolecules* **2021**, *54*, 3810.
[51] M. Safari, C. Ocando, Y. Liao, M. Drechsler, N. Volk, R. Schaller, M. Held, V. Abetz, H. Schmalz, A. Müller, *Polymer* **2024**, *298*, 126863.
[52] A. J. Müller, Z. H. Hernández, M. L. Arnal, J. J. Sánchez, *Polym. Bull.* **1997**, *39*, 465.
[53] M. L. Arnal, V. Balsamo, G. Ronca, A. Sánchez, A. J. Müller, E. Cañizales, C. Urbina de Navarro, *J. Therm. Anal. Calorim.* **2000**, *59*, 451.
[54] A. J. Müller, M. L. Arnal, *Prog. Polym. Sci.* **2005**, *30*, 559.
[55] L. Sangroniz, B. Wang, Y. Su, G. Liu, D. Cavallo, D. Wang, A. J. Müller, *Prog. Polym. Sci.* **2021**, *115*, 101376.
[56] A. Gałeski, Z. Bartczak, M. Pracella, *Polymer* **1984**, *25*, 1323.
[57] Z. Bartczak, A. Galeski, N. P. Krasnikova, *Polymer* **1987**, *28*, 1627.
[58] B. O. Reid, M. Vadlamudi, A. Mamun, H. Janani, H. Gao, W. Hu, R. G. Alamo, *Macromolecules* **2013**, *46*, 6485.
[59] X. Chen, A. Mamun, R. G. Alamo, *Macromol. Chem. Phys.* **2015**, *216*, 1220.

